



Thermal Fatigue Behavior of Thick and Porous Thermal Barrier Coatings Systems

A. Scrivani, G. Rizzi, U. Bardi, C. Giolli, M. Muniz Miranda, S. Ciattini, A. Fossati, and F. Borgioli

(Submitted February 28, 2007; in revised form August 10, 2007)

High-temperature thermal fatigue causes the failure of thermal barrier coating (TBC) systems. This paper addresses the development of thick TBCs, focusing on the microstructure and the porosity of the yttria partially stabilized zirconia (YPSZ) coating, regarding its resistance to thermal fatigue. Thick TBCs, with different porosity levels, were produced by means of a CoNiCrAlY bond coat and YPSZ top coat, both had been sprayed by air plasma spray. The thermal fatigue resistance of new TBC systems and the evolution of the coatings before and after thermal cycling was then evaluated. The limit of thermal fatigue resistance increases depending on the amount of porosity in the top coat. Raman analysis shows that the compressive in-plane stress increases in the TBC systems after thermal cycling, nevertheless the increasing rate has a trend which is contrary to the porosity level of top coat.

Keywords coatings for gas turbine components, thermal barrier coatings, thermal cycling fatigue resistance, yttria partially stabilized zirconia

1. Introduction

Thermal barrier coatings (TBCs) are applied on gas turbine and aeronautical engine components in order to improve their hot corrosion and oxidation resistances and their service lifetime through a reduction of the service temperature. The TBC systems consist of a duplex structure made up of a metallic MCrAlY (M stands for either Co, Ni, or Fe or a combination of these elements) bond coat and yttria partially stabilized zirconia (YPSZ) ceramic top coat. The bond coat is typically deposited by means of either vacuum plasma spraying (VPS), air plasma spraying (APS), or high-velocity oxy-fuel (HVOF) processes; the YPSZ top coat is typically deposited by an electron beam physical vapor deposition (EB-PVD) process or by an APS process (Ref 1-3). The bond coat

This article is an invited paper selected from presentations at the 2007 International Thermal Spray Conference and has been expanded from the original presentation. It is simultaneously published in *Global Coating Solutions, Proceedings of the 2007 International Thermal Spray Conference*, Beijing, China, May 14-16, 2007, Basil R. Marple, Margaret M. Hyland, Yuk-Chiu Lau, Chang-Jiu Li, Rogerio S. Lima, and Ghislain Montavon, Ed., ASM International, Materials Park, OH, 2007.

A. Scrivani and **G. Rizzi**, Turbocoating S.p.A., Rubbiano di Solignano, Parma, Italy; **U. Bardi**, **C. Giolli**, **M. Muniz Miranda**, and **S. Ciattini**, Dipartimento di Chimica, Università di Firenze, Firenze, Italy; and **A. Fossati** and **F. Borgioli**, Dipartimento di Ingegneria Civile, Università di Firenze, Firenze, Italy. Contact e-mail: gabrielerizzi@turbocoating.it.

surface, onto which the YPSZ top coat is deposited, has a thin oxide layer that mainly consists of various oxides (NiO, Ni(Cr,Al)₂O₄, Cr₂O₃, Y₂O₃, Al₂O₃). This thin oxide layer creates the adhesion (bonding) between the metallic bond coat and the ceramic top coat (Ref 4). However, during engine operation, another oxide layer forms in addition to the native oxide one. This second layer, which is mainly composed of alumina, is commonly referred to as the “thermally grown oxide” (TGO) and it develops slowly during exposure at elevated temperatures (Ref 5-7). TBC systems have a tendency to fail by spalling or by debonding processes under cyclic high-temperature conditions. The performance of TBCs is affected by thermal expansion mismatch between the ceramic and the metal, thermal stresses generated by the temperature gradients in the TBC, ceramic sintering, phase transformations, corrosive and erosive attack, and residual stresses arising from the deposition process (Ref 8, 9). The growth of thermally grown oxides (mainly alumina) between the bond coat and the top coat layers causes large residual stresses, which lead to the spallation of TBC (Ref 10).

The aims of this work were: (1) to compare the resistance of TBC systems to thermal fatigue in function of the different porosity levels and (2) to observe the evolution of the Raman spectra during the thermal cycles in order to retrieve some parameters related to residual stress of the TBC.

2. Experimental

Hastelloy X metal discs (diameter: 25 mm; thickness: 3 mm) were used as substrates for this study. The bond coat of the samples was obtained by means of air plasma spray using commercial CoNiCrAlY powder (chemical composition as AMDRY 995) with a grain size distribution

**Table 1 Chemical composition of YPSZ powder used for spraying experiments**

Compounds	Analytical results (in molar fraction %)
ZrO ₂	Bal.
Y ₂ O ₃	8 ± 1
HfO ₂	max. 2.0
Al ₂ O ₃	max. 0.2
Fe ₂ O ₃	max. 0.3
SiO ₂	max. 0.5
TiO ₂	max. 0.4
CaO	0.03
MgO	<0.01
U+Th	0.04

in the range 45-90 μm ; the thickness of the bond coat was in the range $250 \pm 50 \mu\text{m}$. Furthermore, ceramic coating (top coat) was deposited by air plasma spraying, using a YPSZ commercial powder produced by H.C. Starck with a grain size distribution in the range of 45-125 μm . The composition of the powder is shown in Table 1. The apparent density according to standard ASTM B212 was $2.4 \pm 0.1 \text{ g/cm}^3$. Furnace cycling tests (FCTs) were performed using test equipment consisting of an isothermal static air furnace (type: 3 zone split tube; T_{max} : 1300 °C), a specimen tray in Hastelloy X positioned on a vertical elevator, and a circular tube for forced cooling of specimens when the elevator was lowered. Each thermal cycle in the FCT consist of a 5 min heat up to the steady-state temperature, a 45 min soak at the steady-state temperature, and a 10 min forced air cool down. The chosen steady-state temperature was 1150 °C. According to the original engine manufacturer (OEM) specification, the minimum requested number of thermal cycle to pass the thermal cycling fatigue test is 250 cycles. Metallographic investigation was performed with a metallographic optical microscope Zeiss Axiovert 100A with an image analyzer based on gray contrast, in order to determine: coatings microstructure, coatings thickness, and coatings porosity. Micrographic examination and microprobe analysis were performed by means of ESEM QUANTA 200 FEI with EDAX-ZAF Quantification (Standardless). Raman spectra were recorded using the 514.5 nm line of an Ar⁺ laser, a Jobin-Yvon HG2S monochromator equipped with a cooled RCA-C31034A photomultiplier with a 50 mW laser power. The power density measurements were taken with a power meter instrument (model 362; Scientech, Boulder, CO) giving ~5% accuracy in the 300-1000 nm spectral range. For x-ray diffraction analysis a Philips diffractometer (mod. PW1820) was used in Bragg-Brentano configuration (Cu K α radiation generated at 40 kV and 25 mA). Diffraction patterns were analyzed with the MAUD program using the Rietveld method (Ref 11). The residual stresses were evaluated using the $\sin^2\theta$ method (Ref 12) and additional patterns were collected using a Bruker D8 Advance diffractometer (Cu K α radiation generated at 40 kV and 30 mA). The ψ angle was changed by rotating the incident angle independently of the detector angle. Patterns in the range $2\theta = 60\text{-}80^\circ$ were collected with different ψ angles in the range $-20^\circ \pm 20^\circ$ and the residual stresses were measured

Table 2 Porosity levels of the top coat

Sample type	Porosity level, %
1	16 ± 1
2	21 ± 1
3	29 ± 1

evaluating the interplanar spacing variations of the (220) plane whose peak was at about $2\theta = 74.2^\circ$. In order to take into account the zero error of ψ , which can be due on both instrumental reasons and sample roughness (Ref 13), the data were fitted as a function of ψ and the zero offset value was determined for each sample.

3. Results and Discussion

3.1 Coating Characterization

Microstructures of YPSZ top coat coatings with different porosity levels (as summarized in Table 2) are shown in Fig. 1(a-c); the thickness of the top coat was about 1800 μm for all the sprayed coatings. The phase composition of YPSZ layers was determined by x-ray diffraction analysis and Raman Spectroscopy. X-ray diffraction analysis shows that the coatings essentially consist of tetragonal zirconia (Ref 14). Monoclinic zirconia was not detected in the depth explored by the x-ray beam (Ref 15). Figure 2 shows, as an example, the Raman spectrum of the ceramic top layer of the TBC with a higher porosity (sample 3). The Raman spectra of all the samples show the typical Raman bands for the tetragonal phase of stabilized zirconia coatings (146, 260, 320, 470, 612, 640 cm^{-1}). In fact, the Raman spectrum of tetragonal zirconia (d_{4h}^{15} space group) consist of six lines of the $A1g + 2B1g + 3Eg$ symmetries (Ref 16). This spectrum is characteristic of both pure ZrO₂ and ZrO₂-Ln₂O₃ solid solution (Ln implies the lanthanide series of Y) in the region of 0-8 wt.% of Ln₂O₃ (Ref 17). The Raman spectrum of the tetragonal phase was shown to essentially differ from those of cubic and monoclinic zirconia (Ref 17). The obtained results suggest that the content of monoclinic zirconia, considering the sensibility of the used analytical methods, does not exceed the value of 3%, which is commonly accepted as the upper limit in TBC. The presence of monoclinic phase in TBC has to be avoided because it reduces the TBC lifetime due to the volume increase during the tetragonal to monoclinic transformation.

Residual stresses in the zirconia layer were evaluated before thermal cycling by means of x-ray diffraction analysis using the $\sin^2\psi$ method (Ref 11, 12). The Young's modulus is expected to be affected by coating porosity, which decreases its value in respect to the bulk material (Ref 18). In order to take into account this influence, the Young's modulus was calculated according to the relationship shown by Kroupa (Ref 18), assuming that crack density is negligible and, according to the data of Lackey et al. (Ref 19), the Young's modulus of bulk zirconia is 50 GPa and the Poisson's ratio is 0.25.

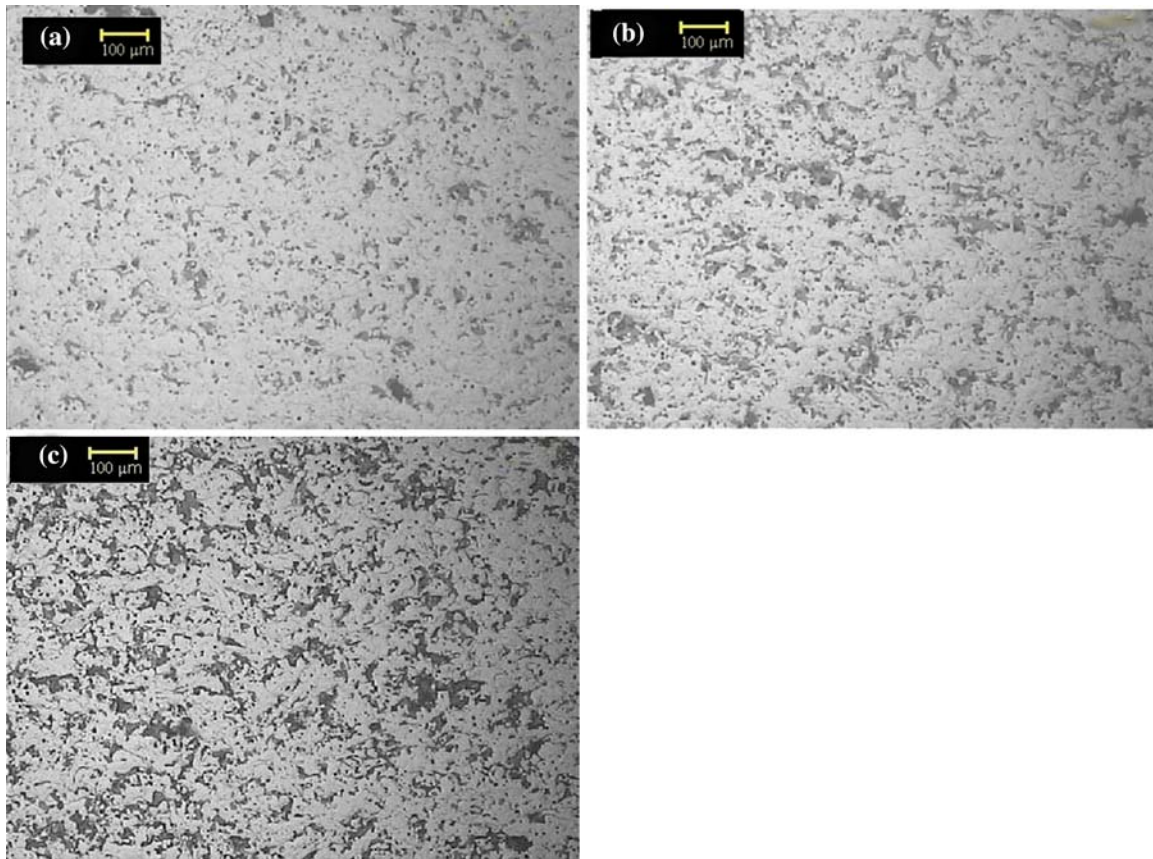


Fig. 1 Optical microscope images of YPSZ top coat of the made TBC systems with increasing porosity level: sample 1 (a), sample 2 (b), and sample 3 (c)

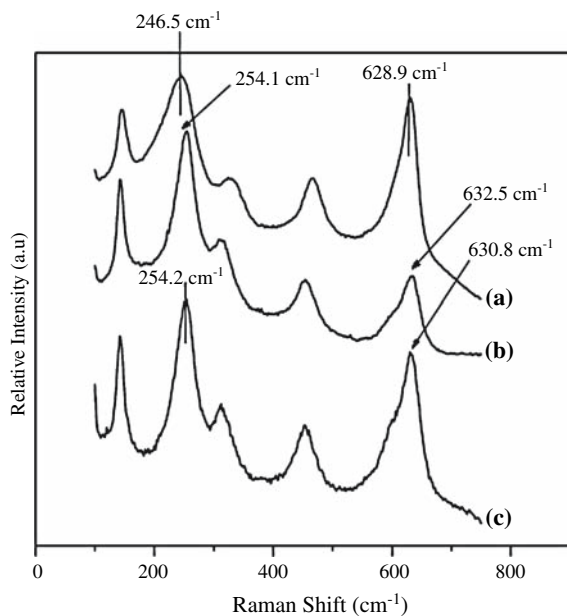


Fig. 2 Raman spectra of sample 3 as-coated (a), 3a 20% spalling at 385 cycles (b), and 3b not delaminated after 455 cycles (c)

The residual stress values for the samples are reported in Table 3. For all the samples compressive stresses are obtained. The samples with lower porosity (1) have a significantly higher residual stress value than those with mean (2) and high (3) porosity, in accordance with the fact that a higher compliance is expected with higher porosity levels. On the other hand, the samples with medium (2) and high (3) porosity show comparable residual stress values. It has to be pointed out that the obtained residual stress values refer to near-surface regions of the coating, due to the low x-ray penetration in zirconia, and they are typically limited to a depth of about 10 μm or more, depending on the porosity. It may be hypothesized that the absence of a decrease of residual stress value for sample 3 in respect to sample 2 may be due to local strain variations, which affect peak shift, and/or porosity variations and the presence of microcracks, which affect Young's modulus value.

3.2 Thermal Fatigue Behavior of Coated Samples

As mentioned previously, according to the applied OEM specification, the minimum requested number of thermal cycles to pass the thermal cycling fatigue test is 250. All the tested samples passed the FCTs (Table 3).

Table 3 Raman stretching modes of Zr-O(II) and Zr-O(I), the difference of Raman stretching modes Zr-O(I) after and before thermal cycling tests, D , and the residual stress values, σ , as obtained by x-ray diffraction analysis

Samples	Sample state	Raman stretching modes of Zr-O(I), cm^{-1}	D	σ , MPa
1	As-coated	629.6		-260 ± 30
1a	Failure after 305 cycles (back side delaminated top coat)	643.3	4.7	
1a	Failure after 305 cycles (front side delaminated top coat)	630.9	1.3	
1b	Failure after 410 cycles (back side delaminated top coat)	635	5.4	
1c	No cracking at 478 cycles	635.7	6.1	
2	As-coated	630		-120 ± 10
2a	Failure after 380 cycles	633.7	3.7	
2b	Failure after 430 cycles	635.4	5.4	
2c	No failure after 455 cycles	632.7	2.7	
3	As-coated	628.9		-130 ± 20
3a	Spalling after 385 cycles (front side delaminated top coat)	632.5	3.6	
3a	Spalling after 385 cycles (back side delaminated top coat)	634.4	5.5	
3b	No failure after 455 cycles	631	2.1	
3c	No failure after 455 cycles	630.8	1.9	

After the thermal cycling test no detectable change of the phase composition of the top coat was observed, according to x-ray diffraction analysis and Raman spectroscopy (Fig. 2b, c). The cracking mode is different when YPSZ top coat is produced by either APS or EB-PVD techniques (Ref 20) and it may also be influenced by coating thickness. Normally the thicker TBCs provide a greater temperature drop across the coatings. In addition, the increased thickness of the coating will increase the stored elastic strain energy and hence the energy release rate for a crack (Ref 21). Thus, the failure mechanisms that cause spallation of thick TBCs are expected to be different in some degree from those of the traditional thin TBCs. Failure of thin plasma-sprayed TBCs occurs in most cases by interface delamination due to different thermomechanical properties of the coating and substrate and oxidation of the bond coat (Ref 22-25). In particular, thick TBCs exhibit a worse thermal shock resistance than thin TBCs. The modification of microstructure of the YPSZ top coat, as introducing a higher porosity level, can increase the thermal shock resistance (Ref 26, 27). After this initial result, the test was continued in order to find the limits. According to the results of these further tests it could be noted that there is a common trend between the thermal fatigue lifetime of coated thick TBC and the porosity of YPSZ top coat, as shown in Tables 2 and 3. The samples with low porosity ($\sim 16\%$) show the lowest average resistance to thermal cycling. The resistance increases in the medium porosity samples ($\sim 21\%$). Regarding the samples with the highest porosity level ($\sim 29\%$), it is possible to see that two samples are not damaged and the beginning spallation of a third one. The presence of undamaged samples after 455 cycles was observed in samples with low and medium porosity. The not delaminated sample with low porosity after 455 cycles shows the typical structure of the wrinkled TGO due to the in-plane compression stresses during thermal cycling tests (Ref 20) and the presence of numerous cracks at the interface TGO/top coat (Fig. 3a), while the sample with medium porosity after the same number of cycles shows the same waved TGO structure and the coalescence of several cracks at the interface TGO/top coat (Fig. 3b).

The not delaminated sample with high porosity after the same number of cycles shows a less waved structure of the TGO in comparison with the other two samples and the absence of cracks of large dimensions in the interface TGO/top coat, as shown in Fig. 3(c). It suggests that the samples with low and medium porosity failed in the interface TGO/top coat. The samples with high porosity show a different microstructure evolution of TGO after thermal cycling. The less-wrinkled interface BC/TC means that the system, with a high porosity top coat, is able to withstand better the in-plane compression stresses during thermal cycling tests.

3.3 Raman Results

The results of Raman analysis for the YPSZ top coat before and after FCTs are shown in Table 3. Raman spectroscopy shows that after thermal cycling the peaks ascribed to tetragonal zirconia show a shift toward lower wave numbers. The principal Raman bands of zirconia tetragonal phase are at about 260 and 640 cm^{-1} and are related with the stretching modes of Zr-O(II) and Zr-O(I), respectively. The difference between the Raman peaks before and after the FCTs are greater than the evaluated instrumental error that is in the order of $\pm 0.2 \text{ cm}^{-1}$. It was shown that a small shift in the peak positions can be explained by the increase in thermal stresses after thermal shock (Ref 28), so the observed shifts may be due to the presence of different in-plane stress. Considering the Raman band at about 640 cm^{-1} , the sample 3 with high porosity level shows a shift toward lower wave numbers (628.9 cm^{-1}) in comparison with the samples 2 (630 cm^{-1}) and 1 (629.6 cm^{-1}) with medium and low porosity. For the $\text{ZrO}_2\text{-}8\text{Y}_2\text{O}_3$ plasma-sprayed coatings, Teixeira et al. (Ref 28) found a linear relationship between the applied stress and the peak shift and each cm^{-1} shift corresponds to 220 MPa . It is well known that the Raman shifts toward higher wave numbers correspond to an increase in the in-plane compressive residual stresses and, in the inverse order, a tensile residual stress. This fact suggests that with an increased porosity level, the residual stress after thermal spray process decreases, according to the residual

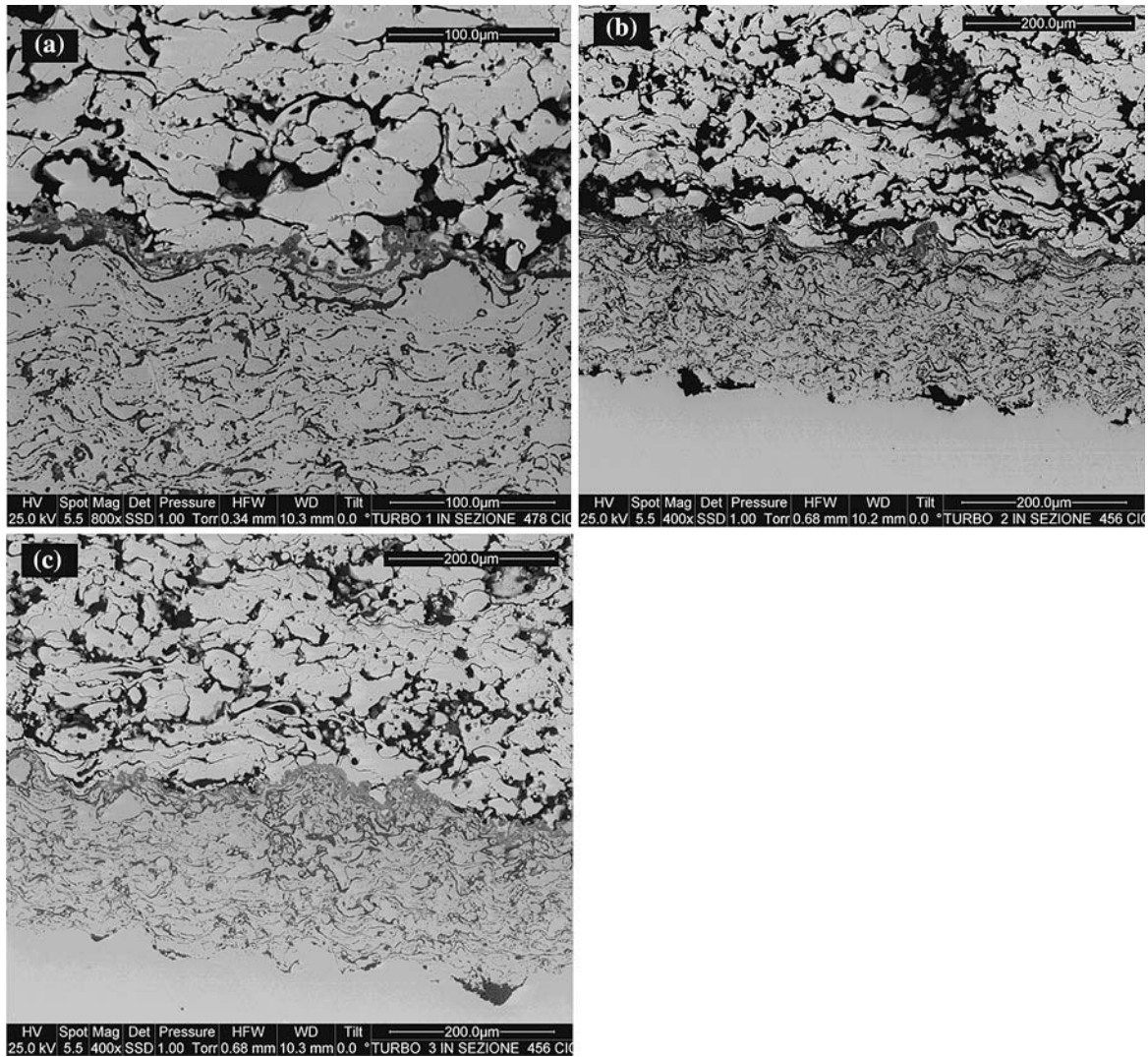


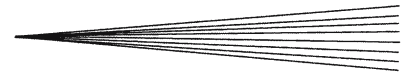
Fig. 3 Back-scattered electron images of the cross section of samples 1c (a), 2c (b), and 3c (c) at the bond coat/TGO/top coat interface

stress evaluation performed with x-ray diffraction analysis. After the thermal cycling tests it is possible to see a general shift to higher values of wave numbers in comparison to the as-coated samples for all the cycled samples, as shown in Table 3. In order to evaluate this shift amount, the difference D of Raman stretching modes Zr-O(I) before and after the thermal cycling tests (in cm^{-1}) was calculated for each kind of sample; the values are shown in Table 3. The average shift for the analyzed samples with low porosity is about 4.3 cm^{-1} , for the samples with medium porosity 3.9 cm^{-1} and for the samples with high porosity is 3.1 cm^{-1} . Supposing that the shift to higher values of the wave numbers is related to the increase of the residual in-plane compressive stress, it is suggested that with an increase in the porosity level the average accumulated stress for the cycled samples decrease. Taking into consideration that the parameter D is, in general, less on the front side of analyzed YPSZ than on the backside after the thermal cycling tests, it is suggested that

there is a stress increase at the interface TGO/top coat during thermal fatigue tests where the TBC systems have failed.

4. Conclusion

TBC systems of different porosity levels with an average thickness of 1.8 mm were produced by APS. The TBCs were characterized and their thermal fatigue behavior was tested. X-ray diffraction analysis and Raman spectroscopy show that the coatings consist essentially of tetragonal zirconia, stabilized by the presence of yttria, and the thermal cycling does not seem to influence the phase composition of the coatings. All the tested samples passed the thermal fatigue test according to the considered OEM procedure, independently of the porosity level. The thermal spray process is, therefore, robust for the FCT



needs. Nevertheless, when looking at the limits of the TBC the thermal fatigue resistance increases with amount of porosity in the top coat. The compressive in-plane stresses of as-coated samples are higher as the porosity content is lower as evaluated by Raman data analysis. After the thermal cycling tests the compressive in-plane stress increases in the TBC systems and it is less a function of the porosity level of top coat. The high content of porosity in the top coat is able to relax the in-phase compressive stress accumulated during thermal cycling and increase the resistance of the porous thick TBC systems.

References

1. W.Brandl, D.Toma, J.Krüger, H.J.Grabke, and G.Matthäus, The Oxidation Behaviour of HVOF Thermal-Sprayed MCrAlY Coatings, *Surf. Coat. Technol.*, 1997, **94-95**, p 21-26
2. D.Toma, W.Brandl, and U.Koster, Studies on the Transient Stage of Oxidation of VPS and HVOF Sprayed MCrAlY Coatings, *Surf. Coat. Technol.*, 1999, **120**, p 8-15
3. E.Lugscheider, C.Herbst, and L.Zhao, Parameter Studies on High-Velocity Oxy-Fuel Spraying of MCrAlY Coatings, *Surf. Coat. Technol.*, 1998, **108-109**, p 16-23
4. E.Y. Lee and R.D. Sisson, The Effect of Bond Coat Oxidation on the Failure of Thermal Barrier Coatings, *Thermal Spray Industrial Application*, C.C. Berndt and S. Sampath, Ed., June 20-24, 1994 (Boston, MA), ASM International, 1994, p 55-59
5. Y. Yaslier and S. Alperine, EB-PVD Thermal Barrier Coatings: Comparative Evaluation and Competing Deposition Technologies, AGARD Report 823, Thermal Barrier Coatings, 1998, p 8-10
6. J.A.Haynes, M.K.Ferber, and W.D.Porter, Thermal Cycling Behavior of Plasma-Sprayed Thermal Barrier Coatings with Various MCrAlX Bond Coats, *J. Thermal Spray Technol.*, 2000, **9**, p 38-43
7. Y.He, K.N.Lee, S.Tewari, and R.A.Miller, Development of Refractory Silicate-Yttria-Stabilized Zirconia Dual-Layer Thermal Barrier Coatings, *J. Thermal Spray Technol.*, 2000, **9**(1), p 59-64
8. J.A.Haynes, E.D.Rigney, M.K.Ferber, and W.D.Porter, Thermal Cycling Behavior of Plasma-Sprayed Thermal Barrier Coatings with Various MCrAlY Bond Coats, *J. Thermal Spray Technol.*, 2000, **9**(1), p 38-48
9. P.Scardi, M.Leoni, and L.Bertamini, Influence of Phase Stability on the Residual Stress in Partially Stabilized Zirconia TBC Produced by Plasma Spray, *Surf. Coat. Technol.*, 1995, **76-77**, p 106-112
10. S.Kuroda and T.W.Clyne, The Quenching Stress in Thermally Sprayed Coatings, *Thin Solid Films*, 2000, **200**, p 49-66
11. L. Lutterotti, S. Matthies, and H-R. Wenk, MAUD (Material Analysis Using Diffraction): A User Friendly Java Program for Rietveld Texture Analysis and More, *Proceedings of the 12th International Conference on Textures of Materials (ICOTOM-12)*, J.A. Szpunar, Ed., Vol. 1, NRC, Ottawa, 1999, p 1599-1604
12. B.D. Cullity, *Elements of X-ray Diffraction*, 2nd ed., Addison-Wesley Publishing, 1978
13. J.Thornton, D.Cookson, and E.Pescott, The Measurement of Strains Within the Bulk of Aged and As-Sprayed Thermal Barrier Coatings Using Synchrotron Radiation, *Surf. Coat. Technol.*, 1999, **120-121**, p 96-102
14. JCPDS card n° 421164, Powder Diffraction File, Joint Committee on Powder Diffraction Standards, International Centre for Diffraction Data, Swarthmore, PA (USA), 1992
15. JCPDS card n° 360420, Powder Diffraction File, Joint Committee on Powder Diffraction Standards, International Centre for Diffraction Data, Swarthmore, PA (USA), 1992
16. D.Michael, Y.Perez, M.Jorba, and R.Collonge, Study by Raman Spectroscopy of Order-Disorder Phenomena Occurring in Some Binary Oxides with Fluorite-Related Structures, *J. Raman Spectrosc.*, 1976, **5**, p 163-180
17. Y.K.Voronko, A.A.Sobol, S.N.Ushakov, and L.I.Tzimbala, Formation of a Tetragonal Structure in Partially Stabilized Zirconia, *Inorg. Mater.*, 1998, **30**, p 747-754
18. F.Kroupa, Nonlinear Behaviour in Compression and Tension of Thermally Sprayed Ceramic Coatings, *J. Thermal Spray Technol.*, 2007, **16**, p 84-95
19. W.J.Lackey, D.P.Stinton, G.A.Cerny, A.C.Schaffhauser, and L.L.Fehrenbacher, Ceramic Coatings for Advanced Heat Engines, A Review and Projection, *Adv. Ceram. Mater.*, 1987, **2**, p 24-30
20. A.G.Evans, D.R.Mumm, J.W.Hutchinson, G.H.Meier, and F.S.Pettit, Mechanisms Controlling the Durability of Thermal Barrier Coatings, *Prog. Mater. Sci.*, 2001, **46**, p 505-511
21. J.W.Hutchinson and Z.Suo, Mixed Mode Cracking in Layered Materials, *Adv. Appl. Mech.*, 1992, **29**, p 63-69
22. E.Tzimas, H.Mülleijans, S.D.Peteves, J.Bressers, and W.Stamm, Failure of Thermal Barrier Coating Systems Under Cyclic Thermomechanical Loading, *Acta Mater.*, 2000, **48**, p 4699-4707
23. G.Qian, T.Nakamura, C.C.Berndt, and S.H.Leigh, Tensile Toughness Test and High Temperature Fracture Analysis of Thermal Barrier Coatings, *Acta Mater.*, 1997, **45**, p 1767-1774
24. J.T.De Masi Marcin, K.D.Sheffler, and S.Bose, Mechanisms of Degradation and Failure in a Plasma-Deposited Thermal Barrier Coating, *ASME J. Eng. Gas Turb. Power*, 1990, **112**, p 521-528
25. A.Rabiei and A.G.Evans, Failure Mechanisms Associated with the Thermally Grown Oxide in Plasma-Sprayed Thermal Barrier Coatings, *Acta Mater.*, 2000, **48**, p 3963-3976
26. R.Morrell, Handbook of Properties of Technical and Engineering Ceramics, Part 1. Her Majesty's Stationery Office, London, UK, 1989
27. R. Vaßen, M. Ahrens, A.F. Waheed, and D. Stover, The Influence of the Microstructure of Thermal Barrier Coating Systems on Sintering and Other Properties *International Thermal Spray Conference*, E. Lugscheider and C.C. Berndt, Eds., March 4-6, 2002 (Essen, Germany), DVS Deutscher Verband für Schweißen, 2002, p 879-883
28. V.Teixeira, M.Andritschky, W.Fischer, H.P.Buchkremer, and D.Stöver, Analysis of Residual Stresses in Thermal Barrier Coatings, *J. Mater. Process. Technol.*, 1999, **92-93**, p 209-221